Ideal near-field thermophotovoltaic cells

Sean Molesky and Zubin Jacob*

Department of Electrical and Computer Engineering, University of Alberta, Edmonton, Alberta, Canada T6G 2V4

(Received 23 October 2014; revised manuscript received 10 March 2015; published 26 May 2015)

We ask the question, what are the ideal characteristics of a near-field thermophotovoltaic cell? Our search leads us to a reformulation of near-field radiative heat transfer in terms of the joint density of electronic states of the emitter-absorber pair in the thermophotovoltaic system. This form reveals that semiconducting materials with narrowband absorption spectra are critical to the energy-conversion efficiency. This essential feature is unavailable in conventional bulk semiconductor cells but can be obtained using low-dimensional materials. Our results show that the presence of matched van Hove singularities resulting from quantum confinement in the emitter and absorber of a thermophotovoltaic cell boosts both the magnitude and spectral selectivity of radiative heat transfer, dramatically improving energy-conversion efficiency. We provide a model near-field thermophotovoltaic system design making use of this idea by employing the van Hove singularities present in carbon nanotubes. Shockley-Queisser analysis shows that the predicted heat transfer characteristics of this model device are fundamentally better than existing thermophotovoltaic designs. Our work paves the way for the use of quantum dots, quantum wells, two-dimensional semiconductors, semiconductor nanowires, and carbon nanotubes as future materials for thermophotovoltaic cells.

DOI: 10.1103/PhysRevB.91.205435 PACS number(s): 84.60.−h, 85.35.Be, 78.20.nd, 81.05.Xj

I. INTRODUCTION

The thermophotovoltaic (TPV) method generalizes the concept of conventional photovoltaics by replacing the source solar spectrum with the thermal emission of an engineered selective emitter [1]. When heated, the emitter is designed to deliver photonic power over a narrow spectral window which can be efficiently converted into electrical power by a matched photovoltaic cell, assumed to be near room temperature. In this way, electrical power can be extracted from any heat reservoir [2,3]. In principle, the TPV approach avoids the two primary loss mechanisms of single-junction solar photovoltaics: the generation of sub-band-gap photons, and the thermalization of excitons with energy much greater than the band gap [4]. For this reason, the theoretical power conversion limitations of TPVs are near that of an ideal heat engine [5,6].

However, in practice, implementation of the TPV idea is difficult. The spectral irradiance of any emitter in the far field is bounded by that of a blackbody with equal temperature [7] (see Fig. 1). For an emitter with temperature below approximately 1000 K, the fraction of emitted power in the range of contemporary low-band-gap photovoltaics (0.4–0.75 eV) is negligible [8], making practical photovoltaic conversion problematic. To overcome this limitation, the emitter of current TPV systems must operate at a temperature between roughly 1200 and 1500 K, creating severe design requirements. Specifically, the emitter must be thermally robust in this temperature range, must suppress emission below the band gap of the photovoltaic cell, which constitutes the majority of the solar spectrum, and must have emissivity near the blackbody limit above the band gap [9,10]. Even without considering temperature-induced degradation of optical properties and structure, current theoretical proposals still require emitter temperatures surpassing 1500 K to reach 40% conversion efficiency under Shockley-Queisser analysis [11–13].

An intriguing prospect to partially alleviate this high-emitter-temperature requirement is to bring the matched emitter and absorber into the near field, where the presence of tunneling photons allows heat transfer to surpass the far-field blackbody limit (near-field thermophotovoltaics, NFTPV [14–16]). Making use of matched near-field resonances [17,18], for example, surface plasmon polaritons [19,20] as in Fig. 1, radiative heat transfer can be made spectrally sharp and significantly greater than the far-field limit (super-Planckian emission [21]).

Nevertheless, basic design issues persist even in theoretical consideration. Analysis of near-field radiative heat transfer has conventionally focused on the maximization of total transferred power, leading naturally to designs using coupled modes of symmetric structures. However, to extract usable electrical power, one half of the near-field resonant architecture must function as a photovoltaic cell. When realistic bulk semiconductors are included as the low-temperature absorber, radiative heat transfer is greatly reduced and spectrally broadened [22,23]. For example, considering a 16-nm gap and identical hypothetical Drude metals with surface plasmon polariton resonances matched to the band gap of gallium antimonide photovoltaic cell [24], replacing the symmetric metal absorber with the photovoltaic cell reduces radiative heat transfer by a factor of nearly 10 (Fig. 1). Furthermore, although the temperature difference between the emitter and the photovoltaic cell can be comparatively reduced, bringing the photovoltaic cell into the near field of the emitter will, in practice, increase its operating temperature and thus will reduce its conversion efficiency [25]. Resultantly, much of the performance gain offered by moving to a near-field thermophotovoltaic systems is lost.

In this paper, we show that the narrowband optical absorption arising from quantum confinement leads to spectrally selective and efficient near-field heat transfer (see Fig. 2). This is a fundamental advantage since absorbed thermal power is the source of exciton generation. Simultaneously, we also uncover the root cause of the poor performance of traditional

*zjacob@ualberta.ca

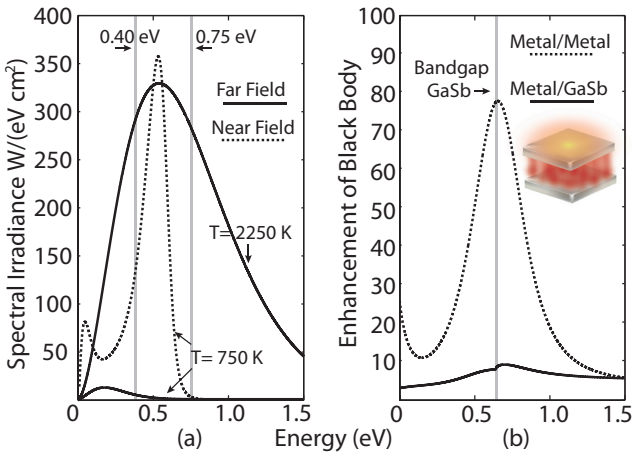

FIG. 1. (Color online) (a) Comparison of radiative heat transfer between the near field and far field calculated using (1). The near-field system consists of two half spaces with optical response of a hypothetical Drude metal, one at 750 K and the other at 0 K, with 0.08 eV loss parameter, 0.58 eV plasma frequency, multiplicative background permittivity of 6, and an additional static imaginary permittivity of 1, separated by a 16-nm gap. This arrangement is shown schematically as an inset in (b). The vertical gray lines mark an approximate range of current single-junction low-band-gap photovoltaics. The enhancement of radiative heat transfer through evanescent modes relaxes the necessity of maintaining the emitter at extremely high temperature. (b) Comparison of the enhancement of radiative heat transfer beyond the blackbody limit for half spaces separated by a 16-nm gap, shown schematically as an inset. The enhancement is temperature independent. The dashed curve is found by assuming identical hypothetical Drude metals with 0.21 eV loss parameter, 0.83 eV plasma frequency, multiplicative background constant of 6, and an additional static imaginary permittivity of 2.5. The solid curve results when one of the metal half spaces is replaced by a gallium antimonide photovoltaic cell. The inclusion of the bulk photovoltaic cell greatly reduces the enhancement effects provided by operating in the near field.

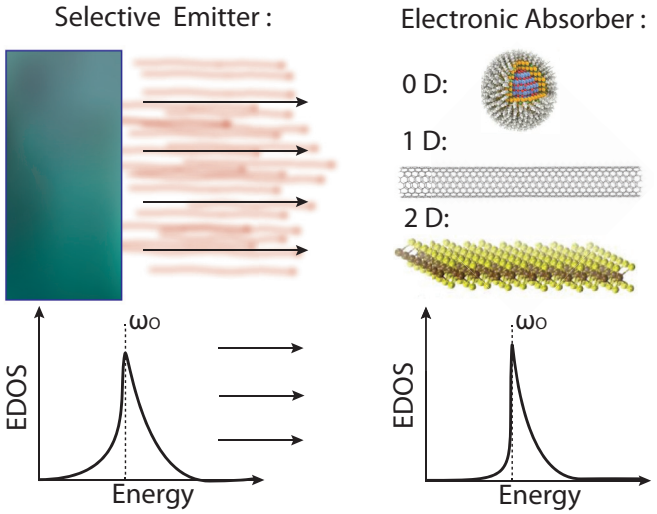

FIG. 2. (Color online) Schematic illustration of the central result of this paper. Here, EDOS stands for the joint density of electronic states. We will show that by matching peaks in the joint density of electronic states of the emitter to peaks in the joint density of electronic states of the photovoltaic cell the spectral selectivity of near-field radiative heat transfer and efficiency of near-field thermophotovoltaics can be greatly improved.

bulk semiconductor photovoltaic cells in the near field by recasting near-field radiative heat transfer in terms of the joint density of electronic states. Appealingly, this result requires only simple arguments from Shockley-Queisser analysis and the essential Kramers-Kronig optical response constraints. We also provide the basis for an experimentally realizable near-field thermophotovoltaic system making use of carbon nanotubes and calculate its enhanced performance metrics. Our predictions can be verified by near-field thermal emission spectroscopy, providing a road map for the use of quantum dots, quantum wells, two-dimensional semiconductors, semiconductor nanowires, and carbon nanotubes as the future building blocks of thermophotovoltaic devices.

II. ENERGY CONSIDERATIONS FOR MAXIMAL RADIATIVE HEAT TRANSFER

From the pioneering works of Rytov [26] and Polder and van Hove [27], the spectral irradiance between two planar half spaces separated by a vacuum gap is given by

$$\begin{aligned}\langle Q(T_1,T_2,\omega_o)\rangle &= \frac{\omega_o^2\,|\Theta(T_1,\omega_o)) - \Theta(T_2,\omega_o)|}{4\pi^2c^2}\\ &\times\left(\sum_{j=s,p}\int_0^1 dk_\rho \frac{\left(1-\left|r_1^j\right|^2\right)\left(1-\left|r_2^j\right|^2\right)}{\left|1-r_1^j r_2^j e^{-2i\,k_\perp^v d}\right|^2}k_\rho\right.\\ &\left.+\,4\int_1^\infty dk_\rho \frac{\mathrm{Im}\left[r_1^j\right]\mathrm{Im}\left[r_2^j\right]e^{-2\mathrm{Im}[k_\perp^v d]}}{\left|1-r_1^j r_2^j e^{-2i\,k_\perp^v d}\right|^2}k_\rho\right),\end{aligned} \quad (1)$$

where c is the speed of light in vacuum, $\Theta(T_i,\omega_o)$ is the mean energy-expectation value of the canonical harmonic oscillator at temperature T_i and angular frequency ω_o, d is the vacuum gap separation normalized by the magnitude of the free-space wave vector at ω_o, T_i is the temperature of the ith half space, k_ρ is the parallel component of the wave vector, again normalized by the magnitude of the free-space wave vector at ω_o, r_i^j is the j-polarized reflection coefficient of the ith half space, $k_\perp^v$ is the normalized perpendicular component of the wave vector in the vacuum gap, and $\mathrm{Im}[\cdots]$ is the imaginary part of the enclosed function.

Intuitively, radiative heat transfer between planar half spaces is maximized when the structures are symmetric, and the vacuum gap is made vanishingly small, $d \to 0$. In this limit the integrand of the spectral irradiance, $H(T_1,T_2,\omega_o,k_\rho)$ from Eq. (1), is dominated by the high-momentum p-polarized evanescent contribution, $k_\rho \gg 1$, and is well approximated by the bound form

$$H(T_1,T_2,\omega_o,k_\rho) = \frac{\omega_o^2|\Theta(T_1,\omega_o) - \Theta(T_2,\omega_o)|}{4\pi^2c^2\{1+[\epsilon'(\omega_o)/\epsilon''(\omega_o)]^2\}}k_\rho, \quad (2)$$

with $\epsilon(\omega_o)$ denoting the relative permittivity of both media and the prime and double-prime superscripts marking the real and imaginary parts of the function. To achieve the greatest possible radiative heat transfer between identical media at a given wave vector and frequency, the so-called upper bound of radiative heat transfer per channel [28], the ratio

$$\gamma(\omega_o) := \frac{\epsilon'(\omega_o)}{\epsilon''(\omega_o)} \tag{3}$$

must be made as small as possible. [This condition is antithetical to the plasmonic field-enhancement figure of merit where $\gamma(\omega_o)$ is maximized.]

Applying the Kramers-Kronig relation [29] to the real part of the permittivity, the $\gamma(\omega_o)$ factor can be expressed entirely in terms of $\epsilon''(\omega_o)$ as

$$\gamma(\omega_o) = \frac{1}{\epsilon''(\omega_o)} + \frac{2}{\pi\epsilon''(\omega_o)}\,\mathcal{P}\int_0^\infty d\omega\,\frac{\omega\,\epsilon''(\omega)}{\omega^2-\omega_o^2}. \tag{4}$$

For energy harvesting with semiconductor photovoltaic cells, Shockley-Queisser efficiency analysis can be used to provide constraints to the material parameters which minimize $\gamma(\omega_o)$:

(1) No radiative heat transfer should occur below the band-gap frequency ω_g because it cannot be converted into useful electrical power. Mathematically, this criterion is stated as $\gamma(\omega_o) \to \infty$ for all $\omega_o < \omega_g$, equivalent to $\epsilon''(\omega_o) \to 0$ for all $\omega_o < \omega_g$. The dispersive part of $\gamma(\omega_g)$ then provides an explicitly positive contribution, and its minimization requires $\epsilon''(\omega_o) \to 0$ for all $\omega_o \neq \omega_g$. This restriction on the global absorption characteristics of the media $\epsilon''(\omega_o)$ can be immediately translated into two statements concerning its polarization $\epsilon'(\omega_o)$. First, $\epsilon'(\omega_g) > 0$. Second, the polarization of the media acts as a store for photonic power. From this store the initially transferred power may either be converted into the internal degrees of freedom of the absorber or may return to the emitter, limiting the total transferred power. The larger the polarization of the medium is, the smaller radiative heat transfer will be.

(2) Radiative heat transfer should be made as great as possible at the band-gap frequency, $\epsilon''(\omega_g) \to \infty$. This second requirement for achieving $\gamma(\omega_g) \to 0$ is provided by the fluctuation-dissipation theorem. To maximize radiative heat transfer at ω_g, we require $\epsilon''(\omega_g) \to \infty$ to generate the largest possible thermal currents, the first term in Eq. (4). The balance of these two conditions leads unequivocally to the conclusion that to minimize $\gamma(\omega_g)$, under the above Shockley-Queisser constraints, $\epsilon''(\omega_o)$ must be sharply resonant about ω_g. Strictly, simultaneous minimization of $\gamma(\omega_g)$ and complete suppression of heat transfer for all sub-band-gap frequencies is only possible if $\epsilon''(\omega_o)$ is mathematically equivalent to the Dirac δ distribution, $\epsilon''(\omega_o) \to \delta(\omega_g)$.

The implications of this result to near-field energy harvesting become immediate by recalling the intimate connection between optical dissipation and the joint density of electronic states,

$$\epsilon''(\omega_o) = \frac{e^2}{\pi m_e^2\omega_o^2}\int dS^d\,\frac{|\mathbf{a}_o\cdot\mathbf{p}_{ji}|^2}{|\nabla_{\mathbf{k}}\,\mathcal{E}_{ji}(\mathbf{k})|}, \tag{5}$$

where $\mathbf{a}_o$ denotes the polarization vector of the electromagnetic excitation, $\mathbf{p}_{ji}$ is the matrix element of the momentum operator, ω_o is the angular frequency, $\mathcal{E}_{ji}(\mathbf{k})$ is the constant-energy surface between filled and excited states such that $\mathcal{E}_{ji}(\mathbf{k}) = \hbar\omega_o$, dS^d is the infinitesimal constant-energy-surface element in d dimensions, and e and m_e are the mass and charge of an electron. Applying Eq. (5) to model free-particle semiconductor systems in one, two and three spatial dimension, we recover the well-known energy scaling behaviors $\epsilon''(\omega_o) \propto \sqrt{\hbar\omega_o - E_g}\,(d=3)$, $C\,(d=2)$, and $1/\sqrt{\hbar\omega_o - E_g}(d=1)$, where C is a constant and E_g is the energy of the band gap, matching the behavior of the joint density of electronic states. It is important to note that suppression (enhancement) of electronic states at a given frequency is the key to decreasing (increasing) optical absorption. However, the Kramers-Kronig relation introduces dependence on the global frequency characteristics through the polarization of the medium. Both these factors have to be taken into account in order to minimize the factor governing spectrally selective near-field heat transfer $\gamma(\omega_o)$.

As previously mentioned, the principal method for overcoming the Shockley-Queisser limit in TPV devices is to spectrally tailor the photonic output of the emitter to frequencies just above the band gap of the photovoltaic cell. But in the near field this frequency range also corresponds to the poorest absorption characteristics for a typical bulk semiconductor. Near the band gap the $\sqrt{\hbar\omega_o - E_g}$ scaling of the joint density of electronic states gives rise to both low absorption $\epsilon''(\omega_g)$ and large polarization, which can be seen by the positive contribution of the principal-value part in the Kramers-Kronig relationship $[\epsilon'(\omega_0) = 1 + \frac{2}{\pi}\,\mathcal{P}\int_0^\infty d\omega\,\frac{\omega\,\epsilon''(\omega)}{\omega^2-\omega_o^2}]$. These two factors lead to large $\gamma(\omega_o)$ factors that are detrimental to spectrally selective heat transfer when ω_o is near ω_g (Fig. 1). In short, the usual properties of a three-dimensional semiconductor completely disagree with those required for maximal radiative heat transfer as given by Eq. (2).

In stark contrast, significant suppression of the $\gamma(\omega_o)$ factor can be obtained if the absorption $\epsilon''(\omega_o)$ of the semiconductor cell is strongly peaked at the operating frequency. According to Eq. (5), such optical behavior is achieved when the joint density of electronic states becomes similar to the ideal Dirac distribution at the band gap. Suppression of the electronic states below the operating frequency is necessary to decrease transfer of inefficient sub-band-gap photons, as dictated by Shockley-Queisser analysis. The suppression of states above the band gap is necessary to decrease the polarization of the medium at the band gap, as required by the Kramers-Kronig relations. These features can essentially be obtained through van Hove singularities, which occur in a free-particle model in low spatial dimensions. This evolution is shown in Fig. 3, where the $\gamma(\omega_o)$ factors for free-particle semiconductor systems in one, two, and three dimensions have been calculated. This structure in the density of electronic states and corresponding narrowband absorption behavior is characteristic of semiconductors with quantum-confined spatial dimensions such as quantum dots, nanotubes, and two-dimensional materials. We conclude based on the above analysis that systems possessing these properties are ideally suited for achieving spectrally selective radiative heat transfer and can function as ideal near-field thermophotovoltaic cells.

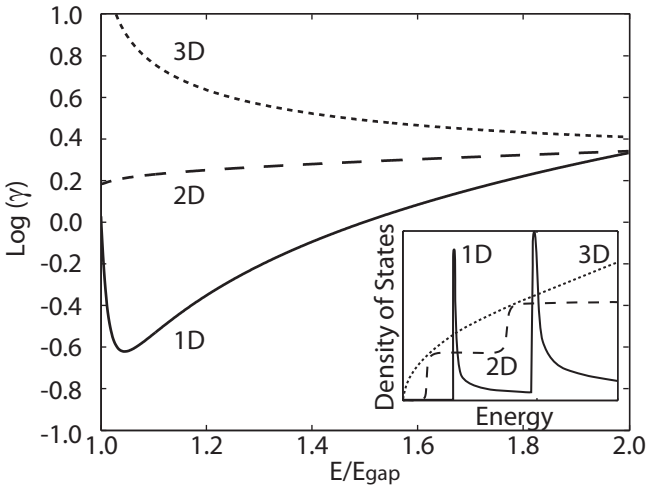

FIG. 3. Base 10 logarithm of the longitudinal $\gamma(\omega_o) := \epsilon''(\omega_o)/\epsilon''(\omega_o)$ factor for one-, two-, and three-dimensional model free-particle semiconductors. The inset shows a schematic illustration of the evolution of the joint density of electronic states for zero, one, and two quantum-confined spatial dimensions characteristic of a semiconductor based on the work of Lee *et al.* [30]. By introducing dimensional constraints the dispersion of the joint density of electronic states can be altered to produce spectrally selective super-Planckian radiative heat transfer near the band gap of a photovoltaic cell. This result illustrates both the primary drawback of employing traditional bulk semiconductor photovoltaics for near-field photonic energy conversion and the usefulness of switching to photovoltaics with quantum-confined dimensions for this application.

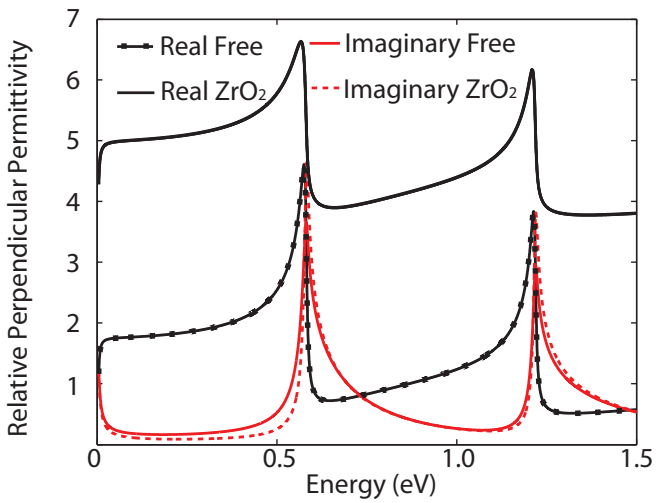

FIG. 4. (Color online) Effective relative permittivity perpendicular to the half spaces for the CNT emitter-absorber pair designed to operate at 1300 K, depicted in Fig. 5. For vacuum gaps on the order of tens of nanometers radiative heat transfer is dominated by tunneling photons with p polarization. In this case, the overall radiative heat transfer properties are primarily determined by the perpendicular permittivity. As predicted by Eq. (2), the radiative heat transfer is maximized when the $\gamma(\omega_o)$ factor is minimized for both the emitter and absorber.

III. MODEL THERMOPHOTOVOLTAIC SYSTEM

A wide body of previous work exists in the areas of photovoltaic cells that utilize materials such as quantum dots, graphene, and carbon nanotubes [31–33]. Our analysis in the previous section shows that any of these low-dimensional material systems are excellent candidates for future near-field TPV cells. Again, we emphasize that the efficiency boost arises from the spectrally selective nature of the absorption in these systems, which is the hallmark of quantum confinement.

As a framework of such a device, we consider here an idealized NFTPV system consisting of an emitter-absorber pair utilizing carbon nanotubes [34] (CNTs) and calculate the radiative-heat-transfer characteristics which can be observed in experiment. Our CNT model device is analogous to the one-dimensional free-particle semiconductor example shown in Fig. 3. The confinement of electrons in CNTs leads to strong van Hove singularities [35], spectrally selective absorption, and semiconductor behavior for specific chiral vectors. Note that nearly identical performance would occur if the CNTs were exchanged for semiconductor nanowires [36]. We have focused on this CNT design, despite current challenges in fabrication and electron-hole pair collection [37], primarily because the thermal robustness [22,38] and low band gap of CNTs seem ideally suited to TPV applications.

Two versions of the CNT system have been considered. The first is designed for a 1300 K emitter and 300 K absorber; the second is for an 800 K emitter and 300 K absorber. In both cases, the absorber is composed of CNTs with chiral vector (19,0) embedded vertically in a matrix of zirconium dioxide on a tungsten backing. This choice of chiral vector allows the CNTs to operate as semiconductors, with a band gap of 0.58 eV. This behavior occurs as the Dirac point of the band structure is avoided [39] due to the angular quantization. The exact current voltage characteristics of the CNT photovoltaic cells have not been included, and instead, ideal p-n junction behavior has been assumed. This is in accordance with the Shockley-Queisser analysis for ideal performance limitations. (To create fully functioning NFTPV cells the CNT on tungsten absorbers must be attached to external electronics and act as the photovoltaic elements [40–42].)

Both emitters are composed of free-standing CNTs with the same chiral vector as the CNTs considered for the absorber and are set on a zirconium dioxide backing. The absorber and emitter are separated from each other by a 16-nm vacuum gap. In the high-temperature case the fill fractions and thickness of the emitter and absorber CNT layers are 65% and 8 nm and 65% and 4 nm, respectively. For the low-temperature case these parameters are altered to 30% and 8 nm and 65% and 16 nm, respectively, in the same order. A schematic of this setup is included as an inset in Fig. 5.

The effective perpendicular permittivities of the two considered designs are shown in Fig. 4. The absorption spikes $\epsilon''(\omega_o)$ can be tuned by varying the chiral vector. The first-principles calculation of these optical properties is based on the Kubo formalism described by Falkovsky and Varlamov [43], with additional loss included via the relaxation-time approximation with an estimated relaxation time of 1 ps [44,45]. The effective parallel permittivities, which play a secondary role in determining the transferred power, are calculated in an identical manner. The main steps of this calculation are

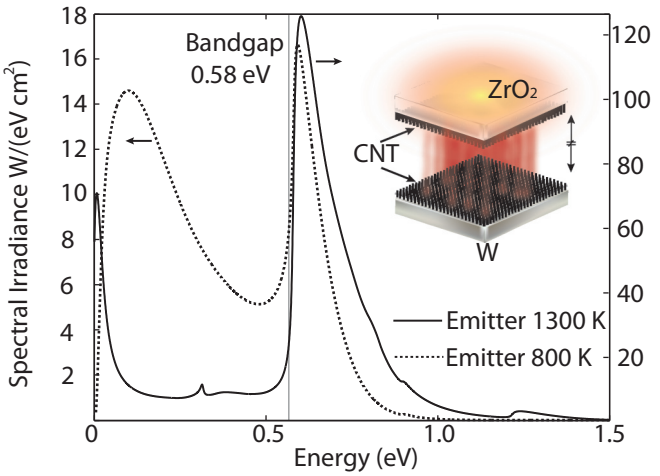

FIG. 5. (Color online) Radiative heat transfer for two metamaterial emitter-absorber pairs utilizing semiconducting CNTs optimized for emitter temperatures of 1300 and 800 K. In both instances the absorber is assumed to be held at a temperature of 300 K. Parameters for the two systems are given in the main text. A schematic of the system is inset over the plot. The greatly enhanced, spectrally thin radiative heat transfer peak produced slightly above the energy band gap of the matched semiconducting CNT absorber seen here is ideal for near-field photonic energy-conversion applications.

outlined in the Appendix. Again, a variety of near-field emitters using other resonances, such as surface plasmon polaritons or phonon polaritons, or absorbers, such as those mentioned above, could also be used with the CNT absorber to obtain very similar results.

In Fig. 5, we plot the spectral irradiance for this CNT-based emitter-absorber system calculated using Rytov's theory. As can be seen by comparing the perpendicular permittivity (Fig. 4) with the spectral irradiance (Fig. 5), the spectral position of peak radiative heat transfer corresponds strongly with the van Hove singularities and the minimization of γ (ω_o). In fact, although the analytical theory of (3) is valid only in the very near field, the spectral position of peak photonic transfer varies only 4% as the vacuum gap is increased up to roughly a tenth of the wavelength of operation, 200 nm.

The spectrally tailored nature of emission and absorption can lead to significant enhancement for energy conversion. Applying Shockley-Queisser analysis [4] as an upper-bound performance estimate, the CNT system with the 1300 K emitter (Fig. 5) could supply up to 15.00 W/cm^2 of electrical power with 53.0% power-conversion efficiency. Likewise, the 800 K emitter system could supply up to 1.07 W/cm^2 of electrical power with 15.6% power-conversion efficiency. For comparison, an optimized conventional bulk gallium antimonide [24] NFTPV design has also been considered. This system consists of a 28-nm-thick Drude metal, with 0.74 eV plasma frequency and 0.21 eV loss parameter, on a tungsten backing with a vacuum-gap separation of 16 nm. Under identical Shockley-Queisser analysis at a 1300 K emitter temperature this conventional system could produce 1.62 W/cm^2 of electrical power with 18.8% power-conversion efficiency, whereas with an emitter temperature of 800 K it could create only 0.01 W/cm^2 of electrical power with 1.6% power-conversion efficiency. More concretely, 73.1% of photonic thermal power transferred from the emitter in the CNT NFTPV device lies above the band gap, 20.7 W/cm^2, for the 1300 K model system, and 25.0%, 1.7 W/cm^2, lies above it in the 800 K model. In comparison, the optimized plasmonic system described above transfers 28.1% of its thermal power above the band gap of the gallium antimonide photovoltaic cell, 2.4 W/cm^2, when the emitter is given a temperature of 1300 K and transfers 3.2%, 0.02 W/cm^2, when the emitter is assumed to have a temperature of 800 K.

IV. SUMMARY

We comment briefly on previous far-field TPV designs which have utilized gallium antimonide [46,47] as the photovoltaic cell for converting the thermal radiation into electric power [48]. Our analysis shows that the optimum cell design for near-field TPV is fundamentally different, and the presence of van Hove singularities in the material comprising the cell is critical for the spectrally selective nature of the transferred energy. This, in turn, should lead to fundamental improvements in energy-conversion efficiency, as shown by the Shockley-Queisser analysis. The implementation of near-field TPV designs is more challenging than implementing far-field TPV designs. However, a fundamental promise of near-field TPV, as mentioned before, is enhanced heat transfer for lower operating temperatures. This arises because the blackbody limit which fundamentally constrains far-field TPV does not apply to near-field TPV, where heat exchange takes place due to the tunneling of evanescent waves.

In summary, we have shown that the ideal joint density of electronic states for near-field photonic energy capture is mathematically equivalent to the Dirac δ distribution. This result immediately reveals why bulk semiconductors are clearly ill suited to near-field photonic energy capture. Switching to photovoltaic cells with van Hove singularities, seen in any semiconductor with a quantum-confined dimension, offers a clear path for improving the efficiency of future NFTPV devices. For experimental verification, we have provided model designs for two such low-dimensional systems consisting of matched metamaterial CNT emitter absorber pairs and have shown that their Shockley-Queisser limit performance metrics are well beyond those achievable with current NFTPV device designs using bulk semiconductor photovoltaics. Our main aim is to emphasize that the absorption characteristics of such low-dimensional materials are ideal for near-field TPV and are an interesting avenue to explore in the development of thermophotovoltaic cells. We hope our work will also motivate future studies to adapt quantum well, quantum dot, two-dimensional semiconductors, and CNT cells specifically for thermophotovoltaics.

ACKNOWLEDGMENTS

This work was supported by funding from the National Science and Engineering Research Council of Canada, Alberta Innovates Technology Futures, and the Helmholtz-Alberta initiative. We also thank C. Cortes and W. Newman for valuable discussions.

APPENDIX: OUTLINE FOR THE CALCULATION OF THE OPTICAL PROPERTIES OF CNTS

As mentioned in the main text, the calculation of the optical properties of the (19,0) chiral vector CNTs used in our sample NFTPV designs has followed the Kubo formalism method described by Falkovsky and Varlamov [43]. The central equation for the dielectric permittivity tensor in this approach is

$$\epsilon_{ab}(k,\omega) = \epsilon_{sur} + \frac{e^2}{hc\epsilon_o}\frac{P_{ab}(k,\omega)}{\omega}, \tag{A1}$$

where

$$P_{ab}(\omega,\mathbf{k}) = \int \frac{dp}{2\pi}\sum_{\omega_n} \mathrm{Tr}[V_a(p)\mathcal{G}(\omega_n,p^+)V_b(p)\mathcal{G}(\omega_n,p^-)]. \tag{A2}$$

Here, P_{ab} denotes the polarization matrix, with the subscripts a and b indicating directions, $\mathcal{G}$ is the Matsubara Green's function, ω is the frequency of the exciting photon, ω_n are the discrete frequencies of the Matsubara sum, Tr is the trace operation, ϵ_o is the permittivity of free space, ϵ_{sur} is the relative permittivity of the surrounding medium, V_a is the velocity operator matrix defined by the Heisenberg operator evolution equation

$$V_a = \dot{x_a} = \frac{[x_a,H]}{i\hbar} = \frac{\partial H}{\partial p_a}, \tag{A3}$$

p is the momentum integration variable, and the and superscript plus and minus symbols indicate the values $p+\frac{k}{2}$ and $p-\frac{k}{2}$, respectively, with k standing for the momentum of the photon excitation. Moreover, the Green's function is explicitly defined as

$$\mathcal{G} = [i\omega_n - H(p)]^{-1}, \tag{A4}$$

and its sum over the discrete frequencies of the Matsubara sum, in terms of its matrix elements indexed by the subscripts i and j, is

$$\sum_{\omega_n}\mathcal{G}_i(\omega_n,p^+)\mathcal{G}_j(\omega_n,p^-) = \frac{f_o(\mathcal{E}_j(p^-)) - f_o(\mathcal{E}_i(p^+))}{\omega + i\eta - [\mathcal{E}_j(p^+) - \mathcal{E}_i(p^-)]}. \tag{A5}$$

In these definitions H is the Hamiltonian of the system, η is the loss parameter following the relaxation-time approximation, and $f_o(\mathcal{E}_j)$ is the Fermi distribution at the energy level of the j-ith eigenstate.

For the carbon nanotube system treated in the text, only π-orbital interactions have been considered due to the energy range of interest [49]. With this approximation the Hamiltonian is

$$H(p,j) = \gamma\left(e^{i\frac{ipa\sqrt{3}}{2} - \frac{i\pi j}{n}} + e^{i\frac{pa}{2\sqrt{3}} + \frac{i\pi j}{n}} + e^{-i\frac{pa}{\sqrt{3}}}\right), \tag{A6}$$

where a is the lattice constant for graphene (2.46 Å), j is the angular momentum number, p is the momentum of the electron along the tube, n is a constant related to the wrapping of the tube [34], and γ is the orbital overlap energy for graphene (3.1 eV). The loss parameter $\eta = h/\tau$ is estimated with a relaxation of 1 ps [44,45] for τ. The energy of the nanotube is similarly defined as

$$\mathcal{E}_j = \pm\gamma\sqrt{1 + 4\cos\left(\frac{\sqrt{3}pa}{2}\right)\cos\left(\frac{j\pi}{n}\right) + 4\cos^2\left(\frac{j\pi}{n}\right)}. \tag{A7}$$

To extend the theory presented by Falkovsky and Varlamov from graphene to the single-layer nanotubes, the Hamiltonian associated with graphene is first enlarged to take into account the energy-level splitting resulting from the additional confinement in the nanotube. This step is accomplished by the substitution

$$\begin{bmatrix} 0 & H \\ H^* & 0 \end{bmatrix} \rightarrow \begin{bmatrix} 0 & 0 & 0 & H_{\mathcal{E}1} \\ 0 & 0 & H_{\mathcal{E}2} & 0 \\ 0 & H^*_{\mathcal{E}2} & 0 & 0 \\ H^*_{\mathcal{E}1} & 0 & 0 & 0 \end{bmatrix}, \tag{A8}$$

with H as above and the $\mathcal{E}_1$ and $\mathcal{E}_2$ subscripts denoting the lowest-level energy bands for the particular chiral vector chosen following the discussion provided by Wong and Akinwande [39]. The velocity operators for axial, z, and angular, θ, directions are then

$$V_z = \begin{bmatrix} 0 & 0 & 0 & v_{Z\mathcal{E}1} \\ 0 & 0 & v_{Z\mathcal{E}2} & 0 \\ 0 & v^*_{Z\mathcal{E}2} & 0 & 0 \\ v^*_{Z\mathcal{E}1} & 0 & 0 & 0 \end{bmatrix} \tag{A9}$$

for the axial direction and

$$V_{\theta+} = \begin{bmatrix} 0 & 0 & v_{\theta\mathcal{E}2} & 0 \\ 0 & 0 & 0 & 0 \\ v^*_{\theta\mathcal{E}2} & 0 & 0 & 0 \\ 0 & 0 & 0 & 0 \end{bmatrix}, \tag{A10}$$

$$V_{\theta-} = \begin{bmatrix} 0 & 0 & 0 & 0 \\ 0 & 0 & 0 & v_{\theta\mathcal{E}1} \\ 0 & 0 & 0 & 0 \\ 0 & v^*_{\theta\mathcal{E}1} & 0 & 0 \end{bmatrix} \tag{A11}$$

for increasing and decreasing angular momentum along the angular direction, respectively (see [34]). Note that for the angular velocity operators the derivative is taken with respect to the natural discrete momenta. These operators are then converted to the eigenbasis of the Hamiltonian by the linear transformation $v \rightarrow U^\dagger v U$, with

$$U = \begin{bmatrix} -\frac{H_{\mathcal{E}1}}{|H_{\mathcal{E}1}|} & 0 & 0 & \frac{H_{\mathcal{E}1}}{|H_{\mathcal{E}1}|} \\ 0 & -\frac{H_{\mathcal{E}2}}{|H_{\mathcal{E}2}|} & \frac{H_{\mathcal{E}2}}{|H_{\mathcal{E}2}|} & 0 \\ 0 & 1 & 1 & 0 \\ 1 & 0 & 0 & 1 \end{bmatrix}. \tag{A12}$$

An identical procedure is undertaken for the effective mass operators, $M_{ij} = \pm\frac{1}{\hbar^2}\frac{\partial^2 H}{\partial p_i \partial p_j}$, for the calculation of the static conductivities used in the relaxation-time approximation. With these substitutions the procedure detailed by Falkovsky and Varlamov [43], equations (A1) and (A2), can be followed directly to achieve Fig. 4.

[1] B. D. Wedlockt, Proc. IEEE **51**, 694 (1963).
[2] R. E. Nelson, Semicond. Sci. Technol. **18**, 141 (2003).
[3] S. Basu, Y. Chen, and Z. M. Zhang, Int. J. Energy Res. **31**, 689 (2007).
[4] W. Shockley and H. Queisser, J. Appl. Phys. **32**, 510 (1961).
[5] N.-P. Harder and P. Würfel, Semicond. Sci. Technol. **18**, S151 (2003).
[6] A. Datas and C. Algora, Sol. Energy Mater. Sol. Cells **94**, 2137 (2010).
[7] J. Greffet and M. Nieto-Vesperinas, J. Opt. Soc. Am. A **15**, 2735 (1998).
[8] P. Bermel, M. Ghebrebrhan, W. Chan, Y. X. Yeng, M. Araghchini, R. Hamam, C. H. Marton, K. F. Jensen, M. Soljačić, J. D. Joannopoulos, S. G. Johnson, and I. Celanovic, Opt. Express **18**, A314 (2010).
[9] E. Rephaeli and S. Fan, Opt. Express **17**, 15145 (2009).
[10] I. Celanovic, N. Jovanovic, and J. Kassakian, Appl. Phys. Lett. **92**, 193101 (2008).
[11] P. Nagpal, S. E. Han, A. Stein, and D. J. Norris, Nano Lett. **8**, 3238 (2008).
[12] S. Molesky, C. J. Dewalt, and Z. Jacob, Opt. Express **21**, A96 (2013).
[13] Y. Nam, Y. X. Yeng, A. Lenert, P. Bermel, I. Celanovic, M. Soljačić, and E. N. Wang, Solar Energy Mater. Solar Cells **122**, 287 (2014).
[14] R. S. DiMatteo, P. Greiff, S. L. Finberg, K. A. Young-Waithe, H. K. H. Choy, M. M. Masaki, and C. G. Fonstad, Appl. Phys. Lett. **79**, 1894 (2001).
[15] A. Narayanaswamy and G. Chen, Appl. Phys. Lett. **82**, 3544 (2003).
[16] M. Laroche, R. Carminati, and J. Greffet, J. Appl. Phys. **100**, 063704 (2006).
[17] P. Ben-Abdallah, K. Joulain, J. Drevillon, and G. Domingues, J. Appl. Phys. **106**, 044306 (2009).
[18] S. Biehs, M. Tschikin, R. Messina, and P. Ben-Abdallah, Appl. Phys. Lett. **102**, 131106 (2013).
[19] O. Ilic, M. Jablan, J. D. Joannopoulos, I. Celanovic, H. Buljan, and M. Soljačić, Phys. Rev. B **85**, 155422 (2012).
[20] S. V. Boriskina, H. Ghasemi, and G. Chen, Mater. Today **16**, 375 (2013).
[21] Y. Guo, C. L. Cortes, S. Molesky, and Z. Jacob, Appl. Phys. Lett. **101**, 131106 (2012).
[22] R. Messina and P. Ben-Abdallah, Sci. Rep. **3**, 1383 (2013).
[23] T. J. Bright, L. P. Wang, and Z. M. Zhang, J. Heat Transfer **136**, 062701 (2014).
[24] S. Adachi, J. Appl. Phys. **66**, 6030 (1989).
[25] M. Francoeur, R. Vaillon, and M. P. Menguc, IEEE Energy Convers. **26**, 686 (2011).
[26] S. Rytov, Y. Kravtsov, and V. Tatarskii, in *Principles of Statistical Radiophysics 3: Elements of Random Fields* (Springer, Berlin, 1984), pp. 109–162.
[27] D. Polder and M. Van Hove, Phys. Rev. B **4**, 3303 (1971).
[28] J. B. Pendry, J. Phys.: Condens. Matter **11**, 6621 (1999).
[29] L. D. Landau, J. Bell, M. Kearsley, L. Pitaevskii, E. Lifshitz, and J. Sykes, *Electrodynamics of Continuous Media* (Pergamon Press, Oxford, 1984), Vol. 8.
[30] S. J. Lee, N. H. Shin, J. J. Ko, M. J. Park, and R. Kümmel, Semicond. Sci. Technol. **7**, 1072 (1992).
[31] A. I. Hochbaum and P. Yang, Chem. Rev. **110**, 527 (2009).
[32] H. Fang, H. Bechtel, E. Plis, M. Martin, S. Krishna, E. Yablonovitch, and A. Javey, Proc. Natl. Acad. Sci. USA **110**, 11688 (2013).
[33] M. J. Shea and M. S. Arnold, Appl. Phys. Lett. **102**, 243101 (2013).
[34] A. Jorio, G. Dresselhaus, and M. S. Dresselhaus, *Carbon Nanotubes: Advanced Topics in the Synthesis, Structure, Properties and Applications*, Topics in Applied Physics Vol. 111 (Springer, Berlin, 2007).
[35] C. L. Cortes and Z. Jacob, Phys. Rev. B **88**, 045407 (2013).
[36] K. B. Arnardottir, O. Kyriienko, M. E. Portnoi, and I. A. Shelykh, Phys. Rev. B **87**, 125408 (2013).
[37] L. Wang, H. Liu, R. M. Konik, J. A. Misewich, and S. S. Wong, Chem. Soc. Rev. **42**, 8134 (2013).
[38] O. Ilic, M. Jablan, J. D. Joannopoulos, I. Celanovic, and M. Soljačić, Opt. Express **20**, A366 (2012).
[39] H.-S. P. Wong and D. Akinwande, *Carbon Nanotube and Graphene Device Physics* (Cambridge University Press, Cambridge, 2010).
[40] D. J. Bindl, A. J. Ferguson, M.-Y. Wu, N. Kopidakis, J. L. Blackburn, and M. S. Arnold, J. Phys. Chem. Lett. **4**, 3550 (2013).
[41] E. Kymakis and G. Amaratunga, Appl. Phys. Lett. **80**, 112 (2002).
[42] M. Freitag, Y. Martin, J. Misewich, R. Martel, and P. Avouris, Nano Lett. **3**, 1067 (2003).
[43] L. A. Falkovsky and A. A. Varlamov, Eur. Phys. J. B **56**, 281 (2007).
[44] C. Köhler, T. Watermann, A. Knorr, and E. Malic, Phys. Rev. B **84**, 153407 (2011).
[45] C. Köhler, T. Watermann, and E. Malic, J. Phys.: Condens. Matter **25**, 105301 (2013).
[46] M. W. Dashiell, J. F. Beausang, H. Ehsani, G. Nichols, D. M. Depoy, L. R. Danielson, P. Talamo, K. D. Rahner, E. J. Brown, S. R. Burger *et al.*, IEEE Trans. Electron Devices **53**, 2879 (2006).
[47] A. Lenert, D. M. Bierman, Y. Nam, W. R. Chan, I. Celanović, M. Soljačić, and E. N. Wang, Nat. Nanotechnol. **9**, 126 (2014).
[48] T. Bauer, *Thermophotovoltaics: Basic Principles and Critical Aspects of System Design* (Springer, Berlin, 2011).
[49] S. Reich, J. Maultzsch, C. Thomsen, and P. Ordejon, Phys. Rev. B **66**, 035412 (2002).